


## Continuum Model Applied to Granular Analogs of Droplets and Puddles

Jean-Christophe Ono-dit-Biot<sup>1</sup>, Tanel Lorand<sup>1</sup>, and Kari Dalnoki-Veress<sup>1,2,\*</sup>

<sup>1</sup>*Department of Physics and Astronomy, McMaster University, 1280 Main Street West, Hamilton, Ontario, L8S 4M1, Canada*

<sup>2</sup>*UMR CNRS Gulliver 7083, ESPCI Paris, PSL Research University, 75005 Paris, France*

 (Received 13 July 2020; revised 28 September 2020; accepted 16 October 2020; published 24 November 2020)

We investigate the growth of aggregates made of adhesive frictionless oil droplets, piling up against a solid interface. Monodisperse droplets are produced one by one in an aqueous solution and float upward to the top of a liquid cell where they accumulate and form an aggregate at a flat horizontal interface. Initially, the aggregate grows in 3D until its height reaches a critical value. Beyond a critical height, adding more droplets results in the aggregate spreading in 2D along the interface with a constant height. We find that the shape of such aggregates, despite being granular in nature, is well described by a continuum model. The geometry of the aggregates is determined by a balance between droplet buoyancy and adhesion as given by a single parameter, a “granular” capillary length, analogous to the capillary length of a liquid.

DOI: 10.1103/PhysRevLett.125.228001

From playing with sand, sugar, or salt, to the large piles that can be observed in an industrial or agricultural context, the formation of granular piles is familiar to all. Granular materials are of particular interest as they can exhibit both liquid or solidlike behaviors [1–3]. Such systems give rise to unusual properties such as a characteristic angle of repose [4,5], clogging through an opening [6,7], intermittent flow and avalanches [8–10], force chains [10–13], and dynamical heterogeneities [1,14–16]. These properties are strongly affected by modifying the interaction between grains; for example, the water added to sand forms interstitial capillary bridges which facilitate adhesion strong enough to build exquisite sand castles [17–19]. The adhesion forces can originate from diverse mechanisms: depletion interactions [20,21], capillary forces [22,23], electrostatic forces [24,25], or simply van der Waals interactions [21,26]. Understanding these interactions and the effects on structure formation impacts a range of fields; for example, colloidal gels can be used as models to understand biological systems [27–33] or geophysical flows [34], and aggregates of dust particles are studied in the context of planet formation [35].

Here, we are specifically interested in piles and aggregates that form at an obstacle. In many cases piles grow in 3D with a characteristic shape defined by the angle of repose. The angle of repose and its dependence on surface roughness [5,36] or the shape of the grains [37] has been extensively studied. Recent studies have shown that even without friction, spheres can pack and exhibit granular properties such as the angle of repose. For example, Ortiz *et al.* [38] observed sandpilelike structures when flowing repulsive colloids against an obstacle in a microfluidic channel. Similar structures were also observed with glass beads colliding on a target where friction cannot be discounted [39]. In another experiment, Shorts and Feitosa [40] defined

an angle of repose when floating bubbles in a container. A feature of both studies with frictionless particles was that the angle of repose was not sustained when the flow was turned off. Lespiat and co-workers [41] showed that the mechanical behavior of granular materials can be extended to assemblies of frictionless bubbles, including the existence of a critical angle at which the assembly transitions from a solidlike to a liquidlike behavior. Finally, nonzero angles of repose have also been reported in numerical simulations of frictionless particles [42,43]. We contrast these granular piles with the familiar spreading of a continuum liquid on a surface. Instead of forming a 3D pile, a liquid droplet grows in 3D as a spherical cap to a maximum height, after which the liquid spreads in 2D as a pancakelike puddle, with a constant height. This height is set by a balance between surface tension and gravity, and of order the capillary length  $\kappa^{-1} = \sqrt{\gamma/\rho g}$  [44], where  $\gamma$  is the surface tension,  $\rho$  is the density of the liquid, and  $g$  the gravitational acceleration.

Here we introduce adhesion between frictionless athermal oil droplets. Droplets are produced one by one and rise by buoyancy to the top of a liquid cell where they accumulate against a horizontal glass surface and form an aggregate. Surprisingly, the aggregate does not assume a 3D sandpilelike structure as is typical of granular materials. Instead, after an initial regime, the height of the aggregate saturates and the aggregate grows in 2D, spreading along the interface. We find that the growth is analogous to the growth of a liquid puddle, and that the shape of the aggregate is determined by a balance between buoyancy and adhesion between the droplets. In analogy with the capillary length of a liquid  $\kappa^{-1}$ , we introduce a “granular” capillary length, which captures the relative importance of the droplet’s buoyancy and adhesion strength in the formation of the aggregates. This granular analog of the

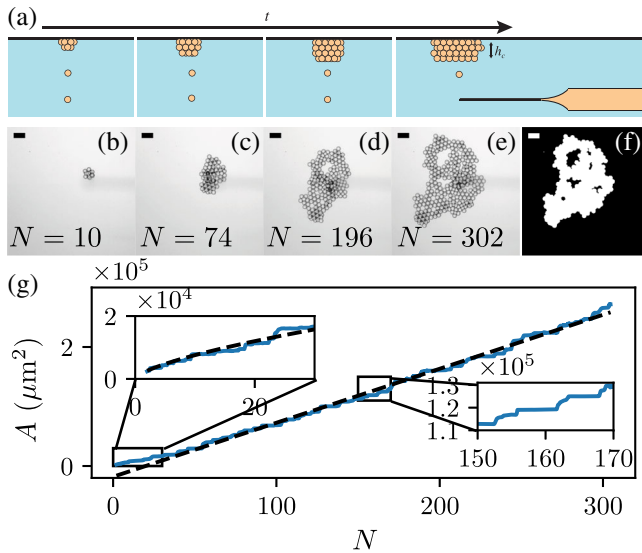


FIG. 1. (a) Schematic side view of the experimental chamber. A glass pipette produces monodisperse oil droplets with a radius of  $\sim 10 \mu\text{m}$  in an aqueous solution. Droplets float to the top and form an aggregate that spreads on the top glass slide over time. (b)–(e) Optical microscopy images of the aggregate at different stage of the growth (scale bars are  $100 \mu\text{m}$ ). (f) Images are binarized to measure the area covered by the droplet aggregate  $A$ . (g) Evolution of the aggregate area as a function of the number of droplets  $N$  (here  $R = 17.8 \mu\text{m}$ ,  $C = 0.10 \text{ mol/l}$ ). The black dashed line is a linear fit of the data for  $N > 30$ . Left inset: early growth of the aggregate with best fit of the model presented in the main text for  $N_{\text{droplets}} \leq 30$ . Right inset: the stepwise increase of the area corresponds to collapsing events.

capillary length is found to well predict the equilibrium shape of the aggregates.

The experimental setup is illustrated in Fig. 1(a) and consists of a chamber ( $55 \times 30 \text{ mm}^2$ ) made from two glass slides separated by a gap of  $2.5 \text{ mm}$  (larger than the size of the droplets by  $10^3$ ). The chamber is filled with an aqueous solution of NaCl at  $1.5\%$  (w/w) and a surfactant sodium dodecyl sulfate (SDS). The concentration of SDS,  $C$ , is varied from  $0.07$  to  $0.21 \text{ mol/l}$  in the experiment. In this concentration range, SDS not only stabilizes the oil droplets, but also forms micelles which act as a depletant resulting in a short-ranged attraction between the droplets [20]. A pipette is inserted into the chamber to produce droplets. The pipette is pulled from a glass capillary tube (World Precision Instruments, U.S.) with a pipette puller (Narishige, Japan) to a tip diameter of  $\sim 10 \mu\text{m}$ . Mineral oil is pushed through the pipette to produce monodisperse droplets, with radius  $R$  using the snap-off instability [45]. The variation in  $R$  within each experimental trial is less than  $1\%$ . The pipette is connected to an open reservoir of mineral oil placed at a fixed height ensuring a constant pressure, and hence a constant volumic flow rate. Because of buoyancy, droplets float to the top of the chamber where they accumulate under the top glass slide [Fig. 1(a)].

Over time, the aggregate grows and spreads horizontally at the top glass slide as illustrated in Fig. 1(a). Droplets are produced a constant rate of about one droplet every  $20 \text{ s}$ . The slow rate ensures that the aggregate has time to rearrange and that the results upon addition of each droplet are quasiequilibrium. The friction between droplets and the top glass slide is negligible and droplets can freely move along the horizontal direction [46]. The chamber is placed atop of an inverted microscope for imaging while the aggregates are growing. The aggregate is a 3D object which is imaged with an optical microscope; thus the images shown in Figs. 1(b)–1(e) are 2D projections. The darker regions show areas where the aggregate has more layers of droplets in the vertical direction, which corresponds to a thicker aggregate. As shown in Fig. 1(e), the aggregates are not always dense and patches without droplets can form within the aggregate. Raw images are analyzed to measure the area covered by droplets  $A$ . Holes within the aggregate are excluded from the measured area, as shown in Fig. 1(f) [47].

The evolution of the area  $A$  as a function of the number of droplets  $N$  in the aggregate is shown in Fig. 1(g). The aggregate does not spread continuously on the glass slide. Rather, the system alternates between droplets which accumulate vertically to some critical height, followed by small avalanches which collapse the aggregate. During the vertical growth the area remains constant while the pressure due to buoyancy grows. Eventually the aggregate reaches a critical height when the pressure cannot be sustained and the structure collapses. These avalanches are accompanied by an increases in the area of the cluster. Alternating between these two stages results in the “avalanche steps” shown in Fig. 1(g) and continues as long as droplets are added to the aggregate.

Figure 1(g) reveals two stages in the evolution of  $A(N)$ . Clearly, for  $N \gtrsim 30$ ,  $A(N)$  is linear, when smoothing over the underlying avalanche steps. Since the change in area is linear in  $N$ , the growth is in 2D with a constant average height  $h_c$ . This linear growth is analogous to the spreading of a liquid puddle once the height of the droplet exceeds a critical value set by  $\kappa^{-1}$  where the area grows linearly with the volume of the liquid. At early stages, for  $N \lesssim 30$ , a deviation from the linear growth is observed in Fig. 1(g). Again this stage is analogous to the growth of a liquid droplet prior to reaching a critical height: just as a droplet grows in all three dimensions as a self-similar spherical cap, the granular system should follow 3D growth with  $A \propto N^{2/3}$ . The 3D growth scaling is verified in the inset of Fig. 1(g) for  $N \leq 30$ , while a best fit line to the 2D growth regime for  $N > 30$  is shown in the main plot. Despite the aggregate being granular in nature, its shape and growth is analogous to that observed with continuous media: an initial 3D growth regime is followed by the aggregate growing horizontally in 2D along the top glass slide [see schematics Fig. 1(a)]. Underlying the two general

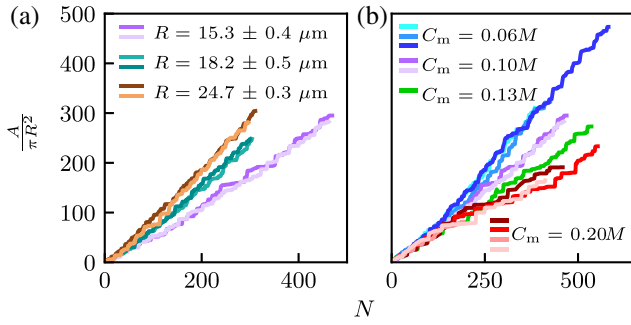


FIG. 2. (a) Normalized aggregate area as a function of the number of droplets for different droplet radii, while the strength of adhesion is kept constant ( $C_m = 0.10$  mol/l). (b) Normalized aggregate area as a function of the number of droplets for different adhesion strengths, while the droplet radius ( $R = 15.3 \pm 0.4 \mu\text{m}$ ) is kept constant. The strength of adhesion increases with SDS concentration. The purple curves correspond to the same data shown in (a).

growth laws are the avalanche steps resulting from the collapsing events, similar to that observed in traditional granular materials.

In order to investigate the role of buoyancy and adhesion, we first consider adjusting the droplet radius while keeping the adhesion between droplets constant. Data for the area of the aggregate normalized by the size of the droplet  $A/\pi R^2$  are shown in Fig. 2(a) for three different radii at a constant concentration of SDS. The uncertainty in the droplet radius originates from the variability from one experimental trial to another. In Fig. 2(a) it is observed that the growth rate increases with droplet radii, and hence buoyancy. In the limit of the puddlelike regime, a faster growth indicates a thinner aggregate with a smaller average critical height of the aggregate  $h_c$ . We now change the strength of adhesion by varying the concentration of SDS while keeping the radius of the droplets (or buoyancy) fixed. A larger volume fraction of micelles in solution leads to stronger adhesion between droplets due to the depletion interaction. The volume fraction of micelles is given by  $\phi_m = (C - C_{\text{CMC}})N_A/N_a$ , with Avogadro's constant  $N_A$ , the critical micelle concentration  $C_{\text{CMC}} = 8$  mM [20], and the number of SDS molecules in one micelle  $N_a \approx 120$  [48]. For simplicity, the control parameter to quantify the adhesion strength is taken as  $C_m = C - C_{\text{CMC}}$  as it is directly proportional to the micelle volume fraction  $\phi_m$ . Figure 2(b) shows the effect of the micelle concentration for a fixed droplet size ( $R = 15.3 \pm 0.4 \mu\text{m}$ ). Thicker aggregates (larger  $h_c$ ) are formed when the strength of adhesion is increased. Thus from Fig. 2 we can conclude that the equilibrium shape of the aggregates is dictated by a balance between buoyancy and adhesion: (i) increasing buoyancy results in thinner aggregates and (ii) increasing adhesion increases the thickness of aggregates.

The balance between buoyancy and adhesion, which determines  $h_c$ , is reminiscent of how the height of a liquid

puddle is governed by a balance between gravity and surface tension given by the capillary length  $\kappa^{-1} = \sqrt{\gamma/\rho g}$  [44]. In the granular system the adhesion  $\mathcal{A}$  ( $\text{J}/\text{m}^2$ ) favors contact between droplets and stabilizes aggregates. Droplets at the surface of the aggregate have a higher free energy as they are missing neighbors in analogy with the definition of surface tension [21]. We can then define a granular capillary length as  $\delta = \sqrt{\mathcal{A}/\Delta\rho g}$ , with  $\Delta\rho$  the difference in density between the aqueous solution and mineral oil. Within a geometrical factor of order one, the height of the aggregate,  $h_c \approx \delta$ . The volume of the aggregate can be written as the product of the volume of one droplet  $V_s$  and the number of droplets,  $V \approx V_s N/\phi$ , where  $\phi$  is the packing fraction of the aggregate. Since  $\phi$  ranges from  $\sim 0.64$  to  $\sim 0.74$  for random-close-packed and hexagonal-close-packed spheres, we take  $\phi \approx 0.7$ . We can approximate that the transition from 3D growth to 2D growth occurs once the aggregate reaches a volume  $V^*$  corresponding to, roughly, a hemisphere with radius  $\delta$ . This crossover corresponds to an aggregate area  $A^* \approx \pi\delta^2$  and characteristic number of droplets  $N^* \approx \phi(V^*/V_s) = (\phi/2)(\delta/R)^3$ . Thus  $N^*$  and  $A^*$  represent the crossover from 3D to 2D growth. In the initial growth regime we have  $A \approx \pi[(3/2\pi)V]^{2/3}$ , which can be renormalized as  $A/A^* \approx (N/N^*)^{2/3}$ . Similarly, for the puddlelike 2D regime, excluding edge effects [49], the volume of the aggregate  $V \approx A\delta$ , which leads to  $A/A^* \approx \frac{2}{3}(N/N^*)$ . To summarize, to within geometric prefactors of order one, there is a crossover from  $A/A^* \propto (N/N^*)^{2/3}$  at early growth of the aggregate to  $A/A^* \propto N/N^*$  at late stages of the growth, with a crossover at  $(A^*, N^*)$ . The parameters  $A^*$  and  $N^*$  depend on the granular capillary length  $\delta$ . To calculate  $\delta$ , and thus  $(A^*, N^*)$ , the adhesion strength  $\mathcal{A}$  due to the depletion force must be measured.

Depletion forces have been shown to scale linearly with the concentration of SDS micelles, proportional to  $C_m$ , and the radius  $R$  [50]. To characterize the droplet-droplet interaction, the adhesion force was measured directly following a method outlined in Ref. [51] as follows. Individual droplets are manipulated using pulled glass micropipettes with modest suction to hold the droplets. The left pipette [see Fig. 3(a)] moves at a constant velocity ( $v = 0.3 \mu\text{m}/\text{s}$ ). The right micropipette is long ( $\sim 1$  cm), thin ( $\sim 10 \mu\text{m}$ ), and bent into an ‘‘L’’ shape so that its deflection (spring constant,  $k = 0.12$  nN/ $\mu\text{m}$ ) can be used to measure the adhesion force. Figure 3(a) shows images of the experiment. The left droplet is initially displaced to the right ( $0 < t < 20$  s). As contact is made,  $t \sim 15$  s, the force sensing pipette deflects to the right and the force increases [Fig. 3(b)]. After keeping the droplets in contact for about 10 s, the motion is reversed and the force decreases  $t > 30$ , eventually becoming negative due to adhesion forces. The contact between droplets is broken when a critical unbinding force  $F_c$  is reached [see Fig. 3(b)] [52].

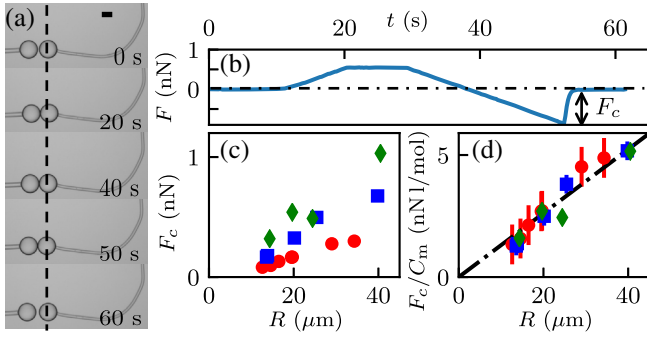


FIG. 3. (a) Adhesion force measurement: two droplets are pushed into contact by the left pipette, held constant, and then pulled apart. The dashed line marks the equilibrium position of the right droplet. The deflection of the sensing pipette (right) is converted to a force. The scale bar is  $100 \mu\text{m}$ . (b) Force measurement between two droplets of oil ( $R = 39.8 \mu\text{m}$ ,  $C_m = 0.13 \text{ mol/l}$ ). The force rises as the droplets are pushed together, and then decreases as the droplets are pulled apart (negative slope). A negative force results from adhesion between the droplets. The contact between droplets is broken when the force suddenly jumps to 0. (c) Unbinding force as a function of the droplet radius for various concentrations in SDS: red circles,  $C_m = 0.06 \text{ mol/l}$ ; blue squares,  $C_m = 0.13 \text{ mol/l}$ ; green diamonds,  $C_m = 0.20 \text{ mol/l}$ . (d) Collapse of the unbinding force by normalizing by the concentration in micelles. The black dashed line corresponds to the linear fit including all three datasets.

Results for  $F_c$  as a function of droplet radius and SDS concentration are shown in Fig. 3(c). The expected normalization of the force  $F_c/C_m$  results in the collapse of the different curves onto a single line [Fig. 3(d)], which confirms  $F_c \propto C_m R$ . Since the unbinding force between two vesicles is  $F_c = \pi R \mathcal{A}$  [53], the slope of the dashed line in Fig. 3(d) is used to obtain the adhesion strength  $\mathcal{A}(C_m)$ . For the system studied here,  $\Delta\rho \approx 200 \text{ kg m}^{-3}$ , and the measured values for  $\delta$  range from  $\sim 36$  to  $\sim 65 \mu\text{m}$ . The crossover values  $(A^*, N^*)$  can now be calculated for each experiment. In Fig. 4 we show the renormalized area  $A/A^*$  as a function of  $N/N^*$  on a double-logarithmic plot. We observe not only an excellent collapse of all the data, but a transition from 3D growth,  $A/A^* \propto (N/N^*)^{2/3}$ , to 2D puddlelike growth at long times,  $A/A^* \propto N/N^*$ , with a crossover at  $(A^*, N^*)$ , as expected from the model.

Here we have explored using a continuum model for an aggregate of athermal droplets, but such liquidlike behaviors have been observed in other granular systems also. For example, a column of glass beads can break up into clusters of grains [54], which is reminiscent of the Plateau-Rayleigh instability observed as a liquid jet breaks into droplets. Analogs to the Rayleigh-Taylor instability have also been reported during the sedimentation of thermal colloids [55]. Other surface-tension-dependent phenomena found at liquid interfaces are capillary fluctuations and capillary waves. Similar fluctuations can be seen at the interface between a granular particle-rich condensed and a

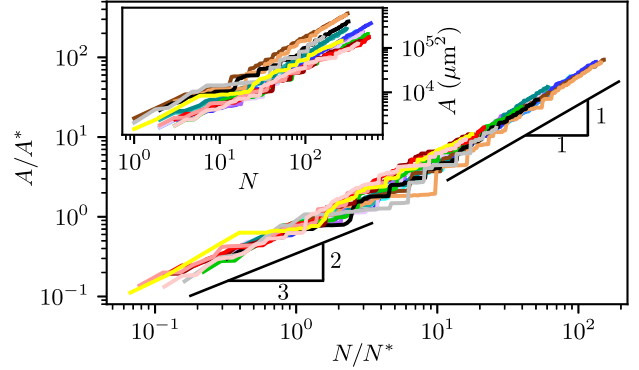


FIG. 4. Double-logarithmic plot of the renormalized aggregate area versus the renormalized number of droplets for various droplet sizes  $R$  and adhesion strength  $\mathcal{A}$ . The aggregate growth transitions from  $(N/N^*)^{2/3}$  to  $N/N^*$  at  $(A^*, N^*)$  (nonrenormalized data shown in inset). The data correspond to those presented in Fig. 2 using the same color code, and three further datasets are included: black ( $R = 24.7 \mu\text{m}$ ,  $C_m = 0.20 \text{ mol/l}$ ), gray ( $R = 24.7 \mu\text{m}$ ,  $C_m = 0.20 \text{ mol/l}$ ), and yellow ( $R = 18.7 \mu\text{m}$ ,  $C_m = 0.20 \text{ mol/l}$ ).

particle-poor gas phase [56–58]. A fundamental advantage of the system described in this study is that the interactions between particles are easily tunable and particles can be imaged and tracked individually. The model is not specific to depletion interactions and can be generalized to other sources of adhesion such as capillary interactions, van der Waals, or biological interactions between cells. Indeed, foams and emulsions have been widely used to model complex biological systems [27–33]. The theoretical framework developed here can be applied to a broad range of systems through defining a granular capillary length, provided that the adhesion  $\mathcal{A}$  can be defined.

While the continuum model presented well explains the growth rate of the aggregate, the model coarse grains the underlying avalanches which result in the discrete growth steps. The literature suggests that the statistics of such discrete events are independent of the length scale of the system [59–62]. The droplet experiment provides an ideal system to study such behaviors and the dependence on the granular capillary length. The noncircular shape of the puddle shown in Fig. 1 is also a direct result of the granular nature of the aggregates not captured by the simple model presented. It is expected that both the avalanche dynamics and shape of the aggregates depends on the granular capillary length; however, these aspects remain outstanding questions.

In summary, we present a study of the growth of an aggregate of adhesive oil droplets. Because of buoyancy forces, the aggregate spreads horizontally along the top surface of the chamber. However, the adhesion between the droplets stabilizes the aggregate along the vertical direction. Aggregates initially grow in 3D until they reach a maximum height, after which the growth occurs in 2D.

This growth is analogous to that of a liquid puddle. The height of the aggregates is entirely determined by the balance between buoyancy and the adhesion strength between droplets. We introduce the granular capillary length,  $\delta = \sqrt{A/\Delta\rho g}$ , the granular equivalent of the capillary length for liquids. Using the analogy with a liquid puddle, we developed a simple model that fully captures the aggregate geometry as a function of the adhesion strength and the droplet size. Despite the aggregates being granular in nature, displaying avalanches in the growth dynamics, the shape of the aggregates can be captured using the physics of continuous media.

We gratefully acknowledge financial support by the Natural Science and Engineering Research Council of Canada. We also thank Karen Daniels, Ramin Golestanian, Johnathan Hoggarth, James Forrest, Elie Raphael, Thomas Salez, An-Chang Shi, and Eric Weeks for discussions.

---

\*dalnoki@mcmaster.ca

- [1] A. D. Gopal and D. J. Durian, Nonlinear Bubble Dynamics in a Slowly Driven Foam, *Phys. Rev. Lett.* **75**, 2610 (1995).
- [2] H. M. Jaeger, S. R. Nagel, and R. P. Behringer, Granular solids, liquids, and gases, *Rev. Mod. Phys.* **68**, 1259 (1996).
- [3] P. Jop, Y. Forterre, and O. Pouliquen, A constitutive law for dense granular flows, *Nature (London)* **441**, 727 (2006).
- [4] C. Coulomb, An attempt to apply the rules of maxima and minima to several problems of stability related to architecture, *Mem. Math. Acad. R. Sci. (Paris)* **7**, 343 (1776).
- [5] B. Andreotti, Y. Forterre, and O. Pouliquen, *Granular Media: Between Fluid and Solid* (Cambridge University Press, Cambridge, England, 2013).
- [6] I. Zuriguel, D. R. Parisi, R. C. Hidalgo, C. Lozano, A. Janda, P. A. Gago, J. P. Peralta, L. M. Ferrer, L. A. Pugnaloni, E. Clément, D. Maza, I. Pagonabarraga, and A. Garcimarin, Clogging transition of many-particle systems flowing through bottlenecks, *Sci. Rep.* **4**, 7324 (2014).
- [7] X. Hong, M. Kohne, M. Morrell, H. Wang, and E. R. Weeks, Clogging of soft particles in two-dimensional hoppers, *Phys. Rev. E* **96**, 062605 (2017).
- [8] V. Frette, K. Christensen, A. Malthe-Sørensen, J. Feder, T. Jøssang, and P. Meakin, Avalanche dynamics in a pile of rice, *Nature (London)* **379**, 49 (1996).
- [9] P.-A. Lemieux and D. J. Durian, From Avalanches to Fluid Flow: A Continuous Picture of Grain Dynamics Down a Heap, *Phys. Rev. Lett.* **85**, 4273 (2000).
- [10] R. Kozłowski, C. M. Carlevaro, K. E. Daniels, L. Kondic, L. A. Pugnaloni, J. E. S. Socolar, H. Zheng, and R. P. Behringer, Dynamics of a grain-scale intruder in a two-dimensional granular medium with and without basal friction, *Phys. Rev. E* **100**, 032905 (2019).
- [11] C.-h. Liu, S. R. Nagel, D. Schecter, S. Coppersmith, S. Majumdar, O. Narayan, and T. Witten, Force fluctuations in bead packs, *Science* **269**, 513 (1995).
- [12] A. A. Zadeh, J. Barés, T. A. Brzinski, K. E. Daniels, J. Dijkstra, N. Docquier, H. O. Everitt, J. E. Kollmer, O. Lantsoght, D. Wang, M. Workamp, Y. Zhao, and H. Zheng, Enlightening force chains: A review of photoelasticimetry in granular matter, *Granular Matter* **21**, 83 (2019).
- [13] Y. Zhao, J. Barés, H. Zheng, J. E. S. Socolar, and R. P. Behringer, Shear-Jammed, Fragile, and Steady States in Homogeneously Strained Granular Materials, *Phys. Rev. Lett.* **123**, 158001 (2019).
- [14] W. K. Kegel and A. van Blaaderen, Direct observation of dynamical heterogeneities in colloidal hard-sphere suspensions, *Science* **287**, 290 (2000).
- [15] A. R. Abate and D. J. Durian, Topological persistence and dynamical heterogeneities near jamming, *Phys. Rev. E* **76**, 021306 (2007).
- [16] X. Cao, H. Zhang, and Y. Han, Release of free-volume bubbles by cooperative-rearrangement regions during the deposition growth of a colloidal glass, *Nat. Commun.* **8**, 362 (2017).
- [17] D. Hornbaker, R. Albert, I. Albert, A.-L. Barabási, and P. Schiffer, What keeps sandcastles standing?, *Nature (London)* **387**, 765 (1997).
- [18] T. G. Mason, A. J. Levine, D. Ertaş, and T. C. Halsey, Critical angle of wet sandpiles, *Phys. Rev. E* **60**, R5044 (1999).
- [19] M. Scheel, R. Seemann, M. Brinkmann, M. Di Michiel, A. Sheppard, B. Breidenbach, and S. Herminghaus, Morphological clues to wet granular pile stability, *Nat. Mater.* **7**, 189 (2008).
- [20] J. Bibette, D. Roux, and B. Pouligny, Creaming of emulsions: The role of depletion forces induced by surfactant, *J. Phys. II* **2**, 401 (1992).
- [21] R. A. L. Jones, R. Jones, R. A. Jones *et al.*, *Soft Condensed Matter* (Oxford University Press, New York, 2002), Vol. 6.
- [22] M. G. Nikolaides, A. R. Bausch, M. F. Hsu, A. D. Dinsmore, M. P. Brenner, C. Gay, and D. A. Weitz, Electric-field-induced capillary attraction between like-charged particles at liquid interfaces, *Nature (London)* **420**, 299 (2002).
- [23] J. C. Loudet, A. M. Alsayed, J. Zhang, and A. G. Yodh, Capillary Interactions between Anisotropic Colloidal Particles, *Phys. Rev. Lett.* **94**, 018301 (2005).
- [24] J. Q. Feng, Electrostatic interaction between two charged dielectric spheres in contact, *Phys. Rev. E* **62**, 2891 (2000).
- [25] U. Konopka, F. Mokler, A. V. Ivlev, M. Kretschmer, G. E. Morfill, H. M. Thomas, H. Rothermel, V. E. Fortov, A. M. Lipaev, V. I. Molotkov, A. P. Nefedov, Y. M. Baturin, Y. Budarin, A. I. Ivanov, and M. Roth, Charge-induced gelation of microparticles, *New J. Phys.* **7**, 227 (2005).
- [26] S. C. Du Pont, P. Gondret, B. Perrin, and M. Rabaud, Wall effects on granular heap stability, *Europhys. Lett.* **61**, 492 (2003).
- [27] K. Guevorkian, M.-J. Colbert, M. Durth, S. Dufour, and F. Brochard-Wyart, Aspiration of Biological Viscoelastic Drops, *Phys. Rev. Lett.* **104**, 218101 (2010).
- [28] O. Lieleg, J. Kayser, G. Brambilla, L. Cipelletti, and A. R. Bausch, Slow dynamics and internal stress relaxation in bundled cytoskeletal networks, *Nat. Mater.* **10**, 236 (2011).
- [29] J. Colombo and E. Del Gado, Stress localization, stiffening, and yielding in a model colloidal gel, *J. Rheol.* **58**, 1089 (2014).
- [30] T. Hayashi and R. W. Carthew, Surface mechanics mediate pattern formation in the developing retina, *Nature (London)* **431**, 647 (2004).

- [31] D. Gonzalez-Rodriguez, K. Guevorkian, S. Douezan, and F. Brochard-Wyart, Soft matter models of developing tissues and tumors, *Science* **338**, 910 (2012).
- [32] L.-L. Pontani, I. Jorjadze, V. Viasnoff, and J. Brujic, Biomimetic emulsions reveal the effect of mechanical forces on cell–cell adhesion, *Proc. Natl. Acad. Sci. U.S.A.* **109**, 9839 (2012).
- [33] S. Douezan and F. Brochard-Wyart, Active diffusion-limited aggregation of cells, *Soft Matter* **8**, 784 (2012).
- [34] D. J. Jerolmack and K. E. Daniels, Viewing earth’s surface as a soft-matter landscape, *Nat. Rev. Phys.* **1**, 716 (2019).
- [35] T. Steinpitz, K. Joeris, F. Jungmann, D. Wolf, L. Brendel, J. Teiser, T. Shinbrot, and G. Wurm, Electrical charging overcomes the bouncing barrier in planet formation, *Nat. Phys.* **16**, 225 (2020).
- [36] N. A. Pohlman, B. L. Severson, J. M. Ottino, and R. M. Lueptow, Surface roughness effects in granular matter: Influence on angle of repose and the absence of segregation, *Phys. Rev. E* **73**, 031304 (2006).
- [37] B.-B. Dai, J. Yang, and C.-Y. Zhou, Micromechanical origin of angle of repose in granular materials, *Granular Matter* **19**, 24 (2017).
- [38] C. P. Ortiz, R. Riehn, and K. E. Daniels, Flow-driven formation of solid-like microsphere heaps, *Soft Matter* **9**, 543 (2013).
- [39] J. Ellowitz, H. Turlier, N. Guttenberg, W. W. Zhang, and S. R. Nagel, Still Water: Dead Zones and Collimated Ejecta from the Impact of Granular Jets, *Phys. Rev. Lett.* **111**, 168001 (2013).
- [40] D. C. Shorts and K. Feitosa, Experimental measurement of the angle of repose of a pile of soft frictionless grains, *Granular Matter* **20**, 2 (2018).
- [41] R. Lespiat, S. Cohen-Addad, and R. Höhler, Jamming and Flow of Random-Close-Packed Spherical Bubbles: An Analogy with Granular Materials, *Phys. Rev. Lett.* **106**, 148302 (2011).
- [42] T. Hatano, Power-law friction in closely packed granular materials, *Phys. Rev. E* **75**, 060301(R) (2007).
- [43] P.-E. Peyneau and J.-N. Roux, Frictionless bead packs have macroscopic friction, but no dilatancy, *Phys. Rev. E* **78**, 011307 (2008).
- [44] P.-G. De Gennes, F. Brochard-Wyart, and D. Quéré, *Capillarity and Wetting Phenomena: Drops, Bubbles, Pearls, Waves* (Springer Science & Business Media, New York, 2013).
- [45] S. Barkley, E. R. Weeks, and K. Dalnoki-Veress, Snap-off production of monodisperse droplets, *Eur. Phys. J. E* **38**, 138 (2015).
- [46] J.-C. Ono-dit-Biot, P. Souillard, S. Barkley, E. R. Weeks, T. Salez, E. Raphael, and K. Dalnoki-Veress, Rearrangement of two dimensional aggregates of droplets under compression: Signatures of the energy landscape from crystal to glass, *Phys. Rev. Research* **2**, 023070 (2020).
- [47] Holes smaller than the projected area of a single droplet are included in the covered area, an overestimate which introduces a small uncertainty, especially as holes are typically observed for large aggregates made of  $\sim 100$  droplets.
- [48] B. L. Bales, L. Messina, A. Vidal, M. Peric, and O. R. Nascimento, Precision relative aggregation number determinations of sds micelles using a spin probe. a model of micelle surface hydration, *J. Phys. Chem. B* **102**, 10347 (1998).
- [49] At early times, near the crossover from 3D to 2D growth, the edge effects cannot be ignored. The edge effects become insignificant as the aggregate grows and the relationship between  $A/A^*$  and  $N/N^*$  is linear.
- [50] A. Vrij, Polymers at interfaces and the interactions in colloidal dispersions, *Pure Appl. Chem.* **48**, 471 (1976).
- [51] M. Backholm and O. Bäumchen, Micropipette force sensors for *in vivo* force measurements on single cells and multicellular microorganisms, *Nat. Protoc.* **14**, 594 (2019).
- [52] See Supplemental Material at <http://link.aps.org/supplemental/10.1103/PhysRevLett.125.228001> for a movie that illustrates the experimental procedure for measuring the strength of adhesion between two droplets.
- [53] F. Brochard-Wyart and P.-G. de Gennes, Unbinding of adhesive vesicles, *C.R. Phys.* **4**, 281 (2003).
- [54] J. R. Royer, D. J. Evans, L. Oyarte, Q. Guo, E. Kapit, M. E. Möbius, S. R. Waitukaitis, and H. M. Jaeger, High-speed tracking of rupture and clustering in freely falling granular streams, *Nature (London)* **459**, 1110 (2009).
- [55] A. Wysocki, C. P. Royall, R. G. Winkler, G. Gompper, H. Tanaka, A. van Blaaderen, and H. Löwen, Direct observation of hydrodynamic instabilities in a driven non-uniform colloidal dispersion, *Soft Matter* **5**, 1340 (2009).
- [56] D. G. Aarts, M. Schmidt, and H. N. Lekkerkerker, Direct visual observation of thermal capillary waves, *Science* **304**, 847 (2004).
- [57] Y. Amarouchene, J.-F. Boudet, and H. Kellay, Capillarylike Fluctuations at the Interface of Falling Granular Jets, *Phys. Rev. Lett.* **100**, 218001 (2008).
- [58] L.-H. Luu, G. Castillo, N. Mujica, and R. Soto, Capillary-like fluctuations of a solid-liquid interface in a noncohesive granular system, *Phys. Rev. E* **87**, 040202(R) (2013).
- [59] J. P. Sethna, K. A. Dahmen, and C. R. Myers, Crackling noise, *Nature (London)* **410**, 242 (2001).
- [60] J. T. Uhl, S. Pathak, D. Schorlemmer, X. Liu, R. Swineman, B. A. Brinkman, M. LeBlanc, G. Tsekenis, N. Friedman, R. Behringer *et al.*, Universal quake statistics: From compressed nanocrystals to earthquakes, *Sci. Rep.* **5**, 16493 (2015).
- [61] R. Benzi, P. Kumar, F. Toschi, and J. Trampert, Earthquake statistics and plastic events in soft-glassy materials, *Geophys. J. Int.* **207**, 1667 (2016).
- [62] P. Kumar, E. Korkolis, R. Benzi, D. Denisov, A. Niemeijer, P. Schall, F. Toschi, and J. Trampert, On interevent time distributions of avalanche dynamics, *Sci. Rep.* **10**, 626 (2020).